Environmental Earth Sciences (2022) 81:208
https://doi.org/10.1007/s12665-022-10322-y

ORIGINAL ARTICLE

A relation for accelerating deformation of sandy soil and its application to predict the time to failure of a sandy model slope under repeated rainfall

Katsuo Sasahara[1]

Received: 3 June 2021 / Accepted: 6 March 2022 / Published online: 25 March 2022

Abstract
The measurement of groundwater level and surface displacement in a sandy model slope under repeated rainfall was conducted to examine the effect of repeated pore pressure loading and unloading on the slope deformation. The velocity increased with small fluctuation even immediately before failure. Positive and negative accelerations occurred due to fluctuations in the velocity. The velocity increased with a considerable rise in the groundwater level and approached its ultimate value immediately before failure. The surface displacement increased not only with the rise in the groundwater level but also with the fall of the groundwater level and under a constant groundwater level. The relationships between the velocity and the absolute value of the acceleration derived from the surface displacement were linear on a logarithmic scale and unique for each stage with increasing and decreasing velocities due to the rise and lowering in the groundwater level. While the relationship was different during the stage of creep during failure. The relationship had been recognized to be applicable only during an increase in velocity; in this paper, a new relationship was established for any velocity trend and the method for predicting the time of failure was proposed based on the relationship between the velocity and acceleration. The time remaining to failure, which was defined as the difference between the predicted failure time and present time, could approach zero at the actual failure time when the constant α in the equation was greater than 1.4, and the determining factor in regression analysis for deriving the constant was high under different periods of measurement before the final event. The time remaining to failure approaching zero might be an indicator for predicting failure time.

Keywords Landslides · Model tests · Displacement · Velocity · Acceleration

Introduction

In humid areas worldwide, many landslides have occurred due to heavy rainfall events, causing substantial damage to human lives or facilities. The mitigation of this damage is a serious problem for man. Early warning systems against rainfall-induced landslides should be established. The prediction of the timing of rainfall-induced landslides based on the measurement of the soil water content, groundwater level and slope displacement can be an effective tool for early warning against such events. In particular, the successful prediction of the failure time of a slope based on the measurement of the displacement along slopes was reported in many studies, such as Saito (1965) and Saito and Yamada (1973) by an extensometer, Crosta and Agliardi (2003) by GPS, Bozzano (2012); Carlà (2019); Mazzanti (2015) by InSAR, and Abraham (2020); Qiao (2020) and Xie (2020) by a tilt sensor. The measurement of the displacement on slopes is often used in practical use for early warning against landslides, such as that performed in Intrieri (2012) and Loew (2017). Most of these studies implemented predicting the failure time of the slope based on the modelling of accelerated displacement prior to slope failure. Saito (1965) reported that the time–strain (or displacement) relationship before soil failure can be divided into the following three stages: (1) primary creep (decelerating creep), (2) secondary creep (steady-state creep) and (3) tertiary creep (accelerating creep). He proposed the time–strain relationships for secondary creep and tertiary creep separately based on measurements of actual landslide movement, creep tests under

✉ Katsuo Sasahara
sasahara@kochi-u.ac.jp

[1] Natural Science Cluster, Kochi University, 2-5-1, Akebonocho, Kochi 780-8520, Japan

constant stress and model slope experiments (Saito and Yamada 1973). The formulae for these types of soil creep relationships have been proposed by many researchers, such as Varns (1982); Voight (1988, 1989); Xiao et al. (2009); Bozzano (2012). Saito (1965) proposed the prediction of the failure time of a slope based on the time–strain relationship. Fukuzono (1985) presented a linear relationship between the logarithms of velocity and acceleration derived from the displacement of a model slope under artificial rainfall with a constant intensity as follows:

$$\frac{dv}{dt} = a \bullet v^{\alpha} \tag{1}$$

Here, v and t are the velocity and time, respectively. a and α are experimental constants and represent the intercept on the vertical axis and the gradient of the expression of the relationship on a logarithmic scale, respectively. The expression of the relationship can be derived through the regression analysis of the velocity and acceleration based on the measured displacement along a slope. He derived the relationship only based on the measurement of the displacement on the model slope under sprinkled water with a constant intensity, which meant monotonically increasing the pore pressure (unloading of total normal stress). This indicates that it was not clear whether the relationship was applicable under a constant stress (secondary creep stage). Voight (1988, 1989) insisted that Eq. (1) was a fundamental physical law for the failure of various materials under constant stress and temperature conditions and developed an equation for rotation and seismic energy release for rock slope failures instead of strain or displacement and for volcanic eruption prediction with geodetic, seismic or geochemical observations. However, it is still unclear under which conditions the relationship can be established due to the availability of few experimental observations. It should be validated based on the experimental data.

Fukuzono (1985) further proposed Eq. (2) below for the failure time of a slope based on this relationship. Integrating Eq. (1) and rearranging the terms produces an equation for deriving the failure time t_r of the slope, as follows:

$$t_r = \frac{v^{1-\alpha}}{a(\alpha - 1)} + t \tag{2}$$

The constants a and α are important when determining the failure time with the equation above. Thus, the relationship between the velocity and acceleration is considered key to predicting failure time. The influence of α on t_r is much greater than that of a because α is exponential for v judging from Eq. (2). This type of prediction method is convenient for practical use because the failure time of a slope can be predicted based on the measurement data of only the displacement of the slope. Equation (3) can be presented as follows:

$$\frac{1}{v} = \left\{a(\alpha - 1)\left(t_r - t\right)\right\}^{\frac{1}{\alpha - 1}} \tag{3}$$

This equation shows that the inverse velocity approaches zero just prior to failure. Many researchers, such as Crosta and Agliardi (2003); Bozzano (2012), and Mazzanti (2015), adopted the inverse velocity as an indicator for predicting the failure time. They were concerned with the scatter of the values of the velocity and acceleration due to the measurement error and tried to minimise the influence of the scatter on the prediction. Hao et al. (2016, 2017) proposed that the ratio of the velocity to the acceleration is a better indicator for predicting failure time with less scatter. It also approached zero immediately before failure according to his examination.

Natural slopes experience many rainfall events. They are subjected to repeated loading and unloading of the pore pressure in the slope; therefore, they undergo substantial changes in stress. Few papers, for example, those by Uchimura (2011) and Sasahara and Sakai (2017), have examined the effect of the repeated loading and unloading of pore pressure on the stress state of a slope. Uchimura (2011) studied sandy soil in a direct shear box with constant shear stress under the conditions of repeated water supply and drainage, and reported that the shear displacement increased with increasing volumetric water contents (hereafter V.W.C.) during the first wetting process but remained approximately constant during subsequent wetting processes until the V.W.C. increased to the maximum during the first wetting stage, and finally developed further with further increases in V.W.C. during the subsequent wetting stage. Sasahara and Sakai (2017) also reported the same types of yielding in the curves of shear strain against suction and surface displacement against the groundwater level (hereafter G.W.L.) for a sandy model slope performed under water sprinkling at a constant intensity. The difference in experimental conditions were recognised by Uchimura (2011) and Sasahara and Sakai (2017). The former was the inclined shear box test under unsaturated conditions, while the latter was the model slope experiment that failed due to a rise in the G.W.L. (in saturated condition). However, the principle of the shear deformation of the soil layer corresponding to the loading and unloading of the pore pressure is the same. Those studies demonstrated the effect of pore pressure preloading by antecedent rainfall on the relationship between the pore pressure and shear strain or between the pore pressure and displacement in the slope. However, the relationship between the pore pressure fluctuation and velocity in a sandy slope has not yet been examined. Moreover, the influence of pore pressure fluctuation on the relationship between the velocity and acceleration is unknown. Under repeated rainfall conditions, failure time

can be predicted in the early stage of displacement if the relationship between the velocity and acceleration is consistent between the former rainfall events. It is more convenient for the practical use of the prediction method.

A review of past literature reveals that the relationship between velocity and acceleration has remained unclear for sandy slopes under repeated rainfall conditions. This paper aims to examine whether the relationship between the velocity and acceleration proposed by Fukuzono can be established during the tertiary creep stage and other stages and then to improve the prediction method based on displacement measurements. Measurements of the G.W.L. and surface displacement along a sandy model slope were conducted under repeated rainfall conditions. Measured data were analysed to examine the relationship between the velocity and acceleration derived from the surface displacement in the studied slope. Finally, the prediction of failure time was implemented by a method based on the examination of the relationship in this paper.

Methodology

Model slope and measurement devices

Measurements of the G.W.L. and the surface displacement of the H21NIED model slope and H23NIED model slope were conducted. Figure 1 shows the geometry of the model slopes and locations of the targets for the extensometers and water level gauges for the H23NIED modelled slope.

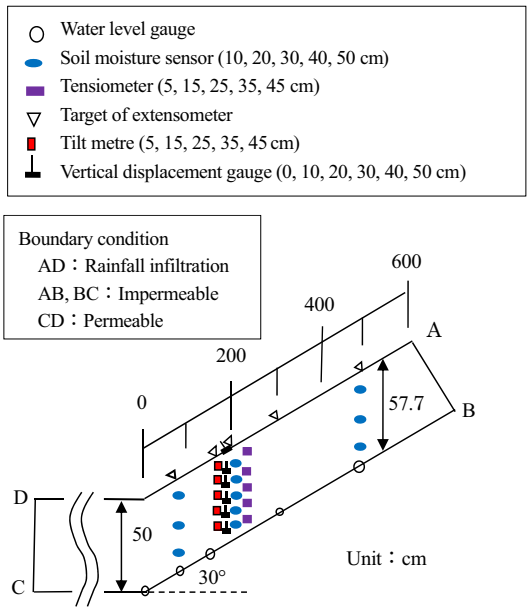

Fig. 1 Model slopes for H23NIED and locations of the measurement instruments

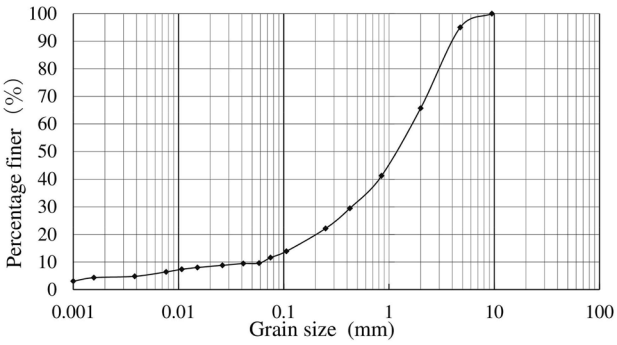

Fig. 2 Grain size distribution of soil

H21NIED model slope also had same geometry while the locations of the targets, measurement devices were different (Sasahara and Sakai 2017). Both model slopes were 300 cm long, 150 cm wide and 50 cm deep (gravitational direction) in a horizontal section; each slope section had a length of 600 cm, a width of 150 cm and a depth of 57.7 cm. The steel flume, with an inclination of 30° and glass walls, and a large-scale rainfall simulator were designed by the National Research Institute for Earth Science and Disaster Resilience, Japan. Vertical blades with a height of 1 cm were located every 50 cm in the longitudinal direction across the base of the flume to prevent slippage between the model and the flume. The upper and side boundaries and base of the flume were impermeable, while the lower boundary at the end of the horizontal flume was permeable. The model slope was composed of granite soil; the grain size distribution, physical and mechanical properties of the soil are given in Fig. 2 and Table 1, respectively. The model slope was compacted horizontally by manual stamping every 20 cm to construct the model slope. Measurement of the wet and dry unit weight of the undisturbed samples extracted from the surface of the slope every 50 cm revealed that the void ratio ranged from 0.652 to 0.678 in the H21NIED model slope and from 0.60 to 0.61 in the H23NIED model slope and that the water content of the soil layer was 3.7–4.4% in the H21NIED model slope and 6.5–7.8% in the H23NIED

Table 1 Physical and mechanical properties of the soil in the model slope

Maximum void ratio of the soil e_{max}	0.947
Minimum void ratio of the soil e_{min}	0.619
Void ratio in the model sliope e	0.652–0.678
Relative density in the model slope Dr (%)	82.1–89.9
Water content in the model slope w (%)	3.7–4.4
Hydraulic conductivity ks (cm/s)	0.0368
Cohesion c′ (Kpa)	0.0
Internal friction angle ϕ' (°)	34.9
Specific gravity of soil mineral G_s	2.658

model slope. The extensometers and water level gauges were installed at the surface and the base of the model slopes, respectively, to measure the surface displacement and G.W.L. The accuracies of the extensometers and water level gauges were 0.01 cm and 0.03–0.05 cm, respectively. A rotating sensor was fixed at the upper boundary of the flume, and an invar wire was connected to the moving rod for the extensometer. The distance of the downward movement of the moving rod was measured by the rotating sensor. The water level gauge contained a pressure sensor in the probe. The soil moisture gauge installed above 5 cm from the water level gauge was used to judge the timing of the termination of artificial rainfall. The soil moisture sensor measures the dielectric constant of the soil and should be calibrated with various volumetric water contents. The calibration factor in the manual was used to derive the volumetric water content in these experiments. The sensor has an accuracy of 0.02 m^3/m^3. The accuracy of tensiometer is 1 kPa.

Experimental conditions

To simulate the stress state in a natural slope that has experienced many rainfall events, preliminary rainfall events were conducted before the targeted rainfall event. For H21NIED, Rains 1 to 3 were preliminary rainfall events, and collapse of the H21NIED slope occurred during Rain 4, as shown in Table 2a; for H23NIED, Rains 1 to 4 were preliminary rainfall events, and collapse of the H23NIED slope occurred during Rain 5, as shown in Table 2b. A constant intensity of rainfall was applied to the model slope until the volumetric water content measured by the soil moisture sensor 5 cm above each water level gauge increased and then remained at a constant value during preliminary rainfall events. The G.W.L., surface displacement and V.W.C. in the slope were measured and recorded automatically every 10 s throughout the test for the H21NIED model slope and every 10–15 s from the start of the rainfall event to the time at which the G.W.L. remained constant after each rainfall event for the H23NIED model slope. The deformation was video recorded from the side of the model slope, and no slip at the base of the flume was observed.

Calculation of velocity and acceleration from measured data

The velocity and acceleration were derived from the measured surface displacement data. The acceleration $(dv/dt)_i$ was derived from two velocities, $dv_{i-1.5}$ and $dv_{i-0.5}$. This derivation requires three surface displacements: sd_{i-2}, sd_{i-1} and sd_i. The increase in the surface displacement and the increment of time are derived in the forms of $(sd_i–sd_{i-1})$ and $(t_i–t_{i-1})$, respectively. Dividing $(sd_i–sd_{i-1})$ by $(t_i–t_{i-1})$ gives the velocity $dv_{i-0.5}$ corresponding to the time $t_{i-0.5}=(t_i–t_{i-1})/2$.

Table 2 Artificial rainfall conditions (a) H21NIED, (b) H23NIED

Event	Intensity (mm/h)	Duration
(a) H21NIED		
Rain 1	30	Oct. 20 11:00:36–14:00:00
Rain 2	30	Oct. 23 9:34:25–11:15:00
Rain 3	15	Oct. 26 9:45:00–12:42:43
Rain 4	30	Nov. 4 11:00:00–15:00:00
(b) H23NIED		
Rain 1	15	Oct. 24 14:10:00–18:37:50
Rain 2	15	Oct. 27 10:27:01–13:26:46
Rain 3	15	Nov. 1 11:01:48–14:01:48
Rain 4	25	Nov. 4 11:06:04–14:05:49
Rain 5	50	Nov. 10 11:17:35–13:49:45

H21NIED: experiments conducted in 2009

H23NIED: experiments conducted in 2011

The acceleration $(dv/dt)_{i-1}$ was derived by dividing the increase in velocity $(dv_{i-0.5}–dv_{i-1.5})$ by the increase in time $(t_{i-0.5}–t_{i-1.5})$.

Experimental results

Variation in measured data with time

Figure 3 shows the variation in the G.W.L., surface displacement, V.W.C., suction and shear strain with time in the H23NIED model slope. The shear strain is derived by multiplying the difference between the initial tilt and present tilt by the length of the gauge (9.2 cm). This variation in the H21NIED model slope was already explained in past literature (Sasahara and Sakai 2017), and the tendency of this variation was almost the same as that of the H23NIED model slope. The G.W.L. rose slightly after Rain 1 and then gradually lowered at 75 cm from the toe of the slope. The G.W.L. rose from the start of each rainfall event, reached a maximum at the termination of the event, then gradually lowered to approximately − 10 cm and finally remained almost constant after the termination of rainfall, especially during Rains 2 to 4, without reaching 450 cm. The G.W.L. remarkably rose until failure during Rain 5 at all locations. It rose to 7.7 cm during Rain 2 and then lowered to -8.1 cm within 87,000 s after the event, rose to 8.8 cm during Rain 3, and then lowered to -7.2 cm within 120,000 s, rose to 10.9 cm during Rain 4 and then lowered to -7.5 cm within 130,000 s at 200 cm. The G.W.L. finally rose to 33 cm at failure during Rain 5. The G.W.L. at 75 cm and 150 cm was higher than that at 200 cm but lower at 300 cm. The G.W.L. did not reach 450 cm, which was positioned near the upper boundary of the flume. The water level gauge could not

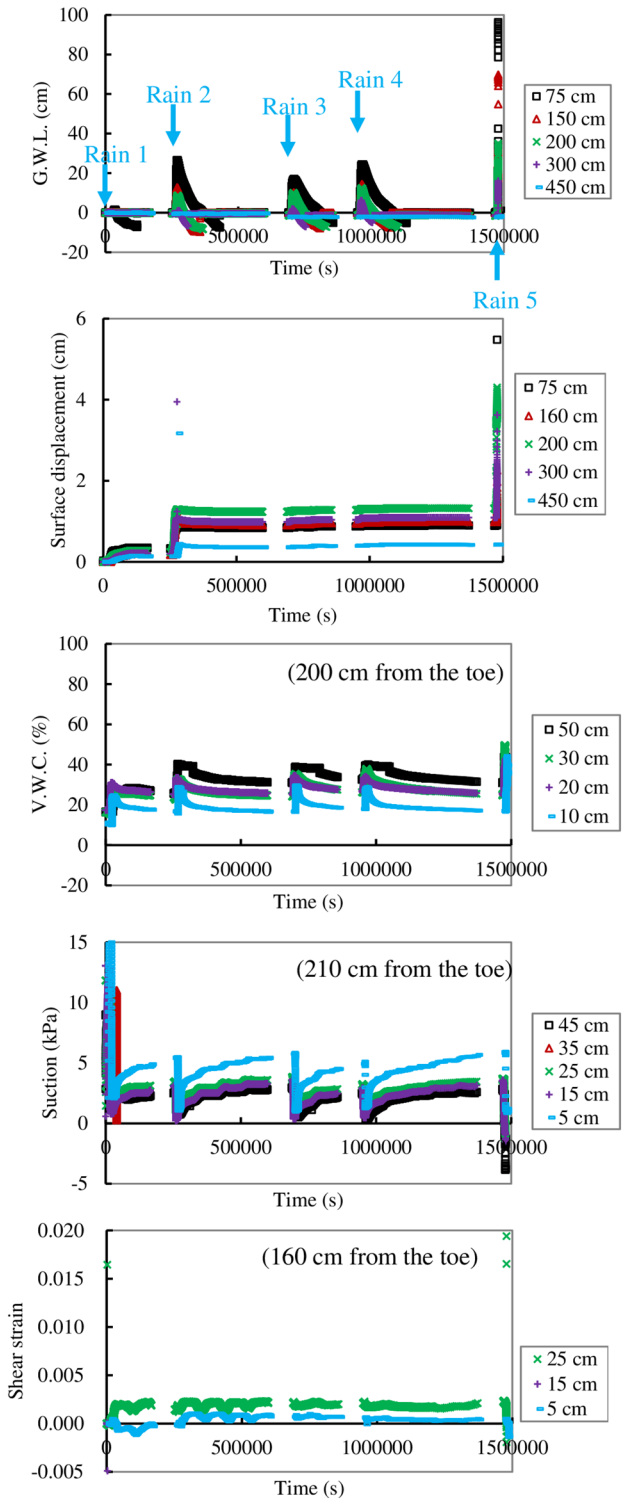

Fig. 3 Variations in the groundwater level and surface displacement with time at different locations on the H23NIED slope model. G.W.L.: groundwater level

measure negative values in principle, so the negative water level data were anomalous. A negative water level was also measured after a rainfall event in the H21NIED model slope and in other sandy model slopes when a pressure sensor-type water level gauge was adopted. Thus, such results might be due to the suction in unsaturated conditions near the base of the slope after the drainage of groundwater.

The surface displacement increased from 0.2 to 0.3 cm after Rain 1 at all locations and then increased during Rain 2. The surface displacement increased to approximately 1.0 cm at 75 cm, 160 cm and 300 cm, to 1.3 cm at 200 cm, and to 0.4 cm at 450 cm. Then, it decreased slightly after Rain 2 and remained almost constant until the start of Rain 5, not changing considerably during Rains 3 and 4. The reason for the constant G.W.L. during Rains 3 and 4 might have been because the maximum G.W.L. during Rains 3 and 4 was lower than that during Rain 2. Sasahara and Sakai (2017) reported that the surface displacement during subsequent rainfall events increased slightly until the G.W.L. reached its maximum during the antecedent rainfall event. The surface displacement might have increased if the G.W.L. during Rains 2 or 3 rose beyond the maximum G.W.L. that occurred during Rain 2. Finally, the surface displacement significantly increased until failure during Rain 5 at all locations. The maximum displacement immediately before failure was 8.0 cm at 75 cm, 7.7 cm at 160 cm, 4.3 cm at 200 cm, 3.6 cm at 300 cm and 0.43 cm at 450 cm.

The V.W.C. increased substantially during the rainfall events and then decreased gradually after the events. The measurement value at 40 cm depth showed repeated fluctuation from 0 to 50%; thus, it was judged to be abnormal; it plotted outside the graph. The rate of the decrease was larger just after the event and then decreased with time to an almost constant value. The V.W.C. at deeper layer was larger than that of the shallower layer. The V.W.C. at 10 cm depth during the event was 25–30%, while it was 16–18% after the drying period (no rainfall period). The V.W.C. in 50 cm during the event was approximately 40%, while it decreased to approximately 30% after the event. It increased significantly beyond the maximum value (25–40%) under antecedent rainfall events until failure at the final rainfall event. The final V.W.C. at each layer was almost the same and ranged from 40 to 45%.

The suction significantly decreased during the rainfall events and increased gradually after the events. In particular, it was more than 10 kPa at first and then decreased to less than 5 kPa at 5 cm depth and approximately 3 kPa (other depths) at Rain 1. The maximum suction at the start of the subsequent rainfall event was approximately 5–6 kPa at 5 cm and 3–4 kPa at other depths, and it increased up to approximately 5 kPa at 5 cm and 3 kPa at other depths. The rate of the increase was larger at first just after the event and then decreased with time. The suction at 5 cm depth was higher. The suction decreased significantly below 0 kPa at every depth corresponding to the saturation of the soil layer during Rain 5.

The shear strain at 35 cm depth and 45 cm depth showed large fluctuations; thus, the measurement at both depths was judged to be incorrect. The shear strains at other depths did not show significant variation from Rain 1 to Rain 4 without small fluctuations. The fluctuation might be due to measurement error. The shear strain at 5 cm depth, 15 cm depth and 25 cm depth decreased largely during Rain 5. This was due to large shear deformation that occurred just prior to the failure of the slope. The shear strain measured at 5 cm, 15 cm and 25 cm in the slope did not indicate significant increase during Rains 1 to 4. It was different from the variation in the surface displacement which increased during rain 2, while the shear strain might have been large at other depths if the measurement of tilt meters at the depths could have been correct.

It should be emphasised that the surface displacement remained constant with the rise in the G.W.L. under Rains 3 and 4. This might be the effect of antecedent rainfall under repeated rainfall conditions.

Variation in velocity, acceleration and G.W.L. with time

Figure 4 shows the variations in the velocity, acceleration and G.W.L. with time during Rain 5 at 200 cm from the toe of the H23NIED mode slope. The surface displacement data were extracted with a difference of more than 0.01 cm from the measured data. The velocity significantly increased from 1,475,700 s to 1,476,000 s (0.017 cm/s) and then decreased until 1,476,300 s. This might be due to the significant rise in the G.W.L. from 4 cm at 1,475,500 s to 11 cm at 1,475,800 s and the gentler increase from 11 cm at 1,475,800 s to 15 cm at 1,476,300 s, respectively. The absolute value of the acceleration also increased and then decreased within those periods. The absolute value of the negative acceleration was of the same magnitude as that of the positive acceleration. This indicates that the velocity repeatedly underwent slight increases and decreases of the same magnitude. The velocity remained almost zero until 1,478,000 s, while the absolute value of the acceleration was approximately 10^{-7} cm/s^2 in this period. The absolute value of the negative acceleration was of the same magnitude as that of the positive acceleration in this period. This slight acceleration might have been due to the repeated slight increases and decreases in velocity. Next, the velocity and acceleration significantly increased until failure at 1,478,655 s. The acceleration was almost positive in this period, which indicates an almost monotonic increase in the velocity, while the G.W.L. showed only a slight increase with time during this period.

The velocity showed a significant increase and decrease from 1,475,700 s to 1,476,300 s, remained near constant (nearly zero) until 1,478,000 s and then significantly increased until failure during Rain 5 at 200 cm in the

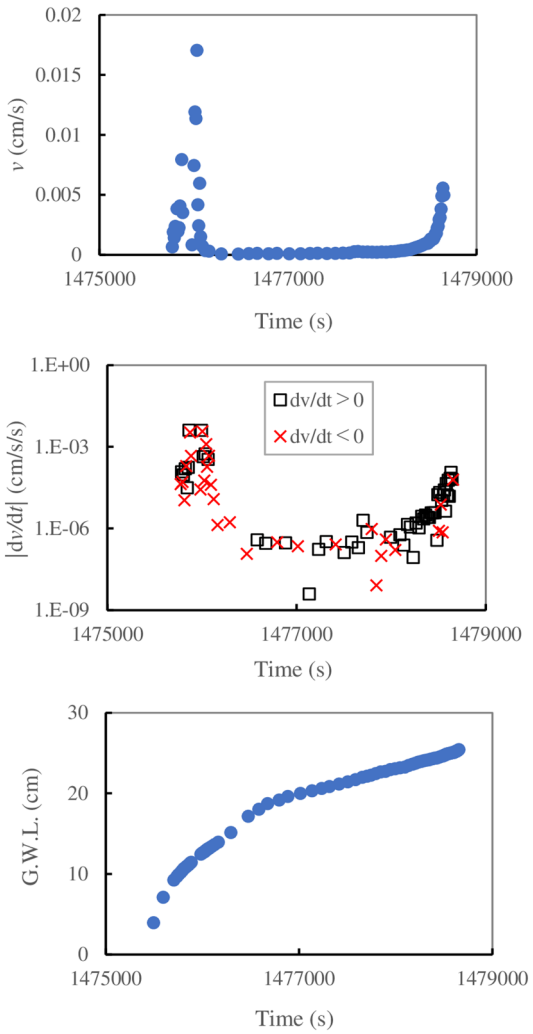

Fig. 4 Variations in the velocity, absolute value of acceleration and groundwater level with time during Rain 5 at 200 cm in the H23NIED model slope. *v* velocity. |d*v*/d*t*| absolute value of acceleration. *G.W.L.* groundwater level

H23NIED model slope. This variation might correspond to the primary creep for the decrease in velocity, the secondary creep for almost constant velocity and the tertiary creep for the final significant increase in velocity. However, the variation in the velocity was not monotonic, and the velocity increased with a small fluctuation in velocity, contrasting the theory of Saito (1965).

Discussion

G.W.L. and velocity to surface displacement

The shear displacement, velocity and G.W.L. only increased significantly during Rains 2 and 5 in the H23NIED model slope within a short time relative to the duration of the entire

experiment, as shown in Fig. 4; therefore, the variation in these metrics with time cannot be clearly shown in graphs. The velocity and G.W.L. versus surface displacement are shown in Fig. 5 to clearly show their variations throughout completed experiments in the H21NIED and H23NIED model slopes. The data were extracted with a difference in the surface displacement of more than 0.01 cm because the accuracy of the extensometer was 0.01 cm.

The relationship between the G.W.L., velocity and surface displacement 300 cm from the toe of the H21NIED model slope are shown in Fig. 5a. The surface displacement increased to 1.5 cm during Rains 1 and 2 without a rise in the G.W.L. (Stage I). The shear deformation of the slope might have proceeded with the suction decrease during and just after Rains 1 and 2. The shear displacement increased slightly from 1.5 to 1.7 cm with the rise in the G.W.L. to 13 cm just after Rain 3 (Stage II); subsequently, the shear displacement slightly progressed from 1.7 to 2.0 cm with the lowering of the G.W.L. (Stage III). The shear displacement increased significantly from 2.0 to 10.0 cm with the second rise in the G.W.L. to more than 30 cm during Rain 4 (Stage IV). The variation in the surface displacement was divided into Stages I to IV according to the loading (rise) and unloading (lowering) of the pore pressure (G.W.L.) in the slope. Notably, the surface displacement increased not only with the rise in the G.W.L. (loading of pore pressure) but also with the lowering of the G.W.L. (unloading of pore pressure). The latter might have been due to the delay in the slope deformation from the pore pressure loading in the slope. The velocity remained almost zero until a surface displacement of 2 cm was reached in Stages I to III. Then, it significantly increased with the significant rise in the G.W.L. and then increased more gently after a surface displacement of 4 cm was reached under a nearly constant G.W.L. The velocity increased with the combination of a significant rise in the G.W.L. and a subsequent constant G.W.L. in this stage. The surface displacement indicated small progress when the G.W.L. was less than the maximum value in previous rainfall event while it increased significantly with the G.W.L. more than the maximum in previous rainfall as mentioned by Sasahara and Sakai (2017). This yielding of the surface displacement against the G.W.L. was one of the effect of antecedent rainfall.

Figure 5b shows the G.W.L. and velocity versus the surface displacement at 200 cm from the toe of the H23NIED model slope. The stage of the increase in the surface displacement was also divided by the rise in and lowering of the G.W.L. The surface displacement increased to 0.6 cm without the generation of the G.W.L. during Rains 1 and 2 (Stage I). The surface displacement started to increase during the middle of Rain 2 and continued to increase after that event to 1.2 cm with the rise in the G.W.L. to 8.6 cm (Stage II). It slightly increased to 1.3 cm with the lowering of the G.W.L.

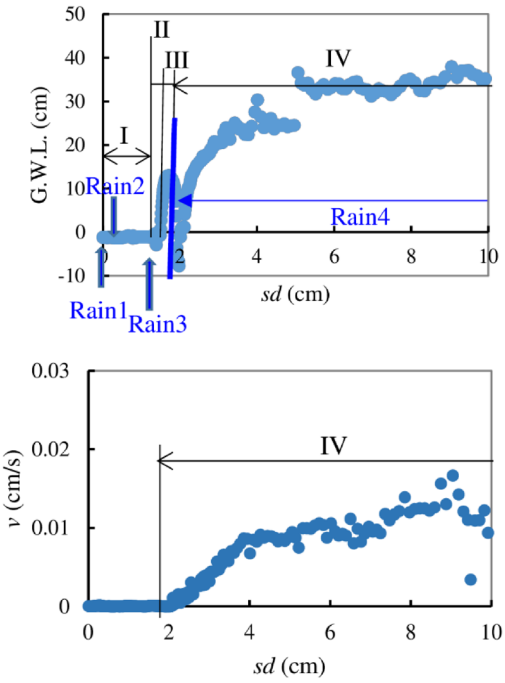

(a) at 300 cm in H21NIED model slope

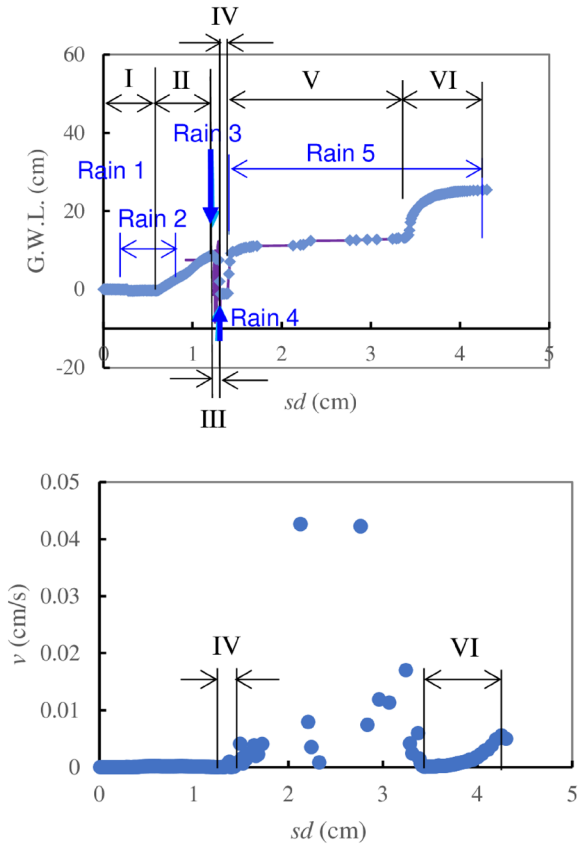

(b) at 200 cm in the H23NIED model slope

Fig. 5 Variations in the groundwater level and velocity with increasing surface displacement in the H21NIED model slope and H23NIED model slope

to − 1.2 cm after Rain 3 (Stage III) and then increased to 1.5 cm with the rise in the G.W.L. to 10.2 cm after Rain 4 (Stage IV). Note the rise in the G.W.L. occurred after Rain 4 in Stage IV. The surface displacement increased to 3.4 cm with a slight rise in the G.W.L. from 10.2 to 13.9 cm during Rain 5 (Stage V). The discontinuous data resulted from large jumps in the surface displacement. Then, the surface displacement increased to 4.3 cm with a significant rise in the G.W.L. to 25.4 cm, as was the case during Rain 5 (Stage VI). The velocity increased after Stage IV, especially during Stage VI, with the combination of a significant rise and subsequent steady state in the G.W.L. The velocity significantly fluctuated during Stage V. The yielding of the surface displacement against the maximum G.W.L. during previous rainfall was also recognized in this model slope.

It should be emphasised that the surface displacement proceeded slightly with the lowering in the G.W.L. during Stage III at 300 cm in the H21NIED model slope and 200 cm in the H23NIED model slope. This was supposed to be caused by the delay of the increase in shear deformation of the soil layer corresponding to viscous-plastic behaviour. The mechanism of the increase in the surface displacement with decreasing G.W.L.s should be examined in near future.

The surface displacement increased larger at Stage IV under constant G.W.L. in H21NIED model slope than at Stage VI under constant G.W.L. in H23NIED model slope. The surface displacement at 300 cm in H21NIED and 200 cm in H23NIED model slopes were 24.8 cm and 4.3 cm both at failure of the slope, respectively. The increase in the surface displacement at Stage IV in H21NIED model slope and Stage VI in H23NIED model slope were 22.8 cm and 1.9 cm, respectively under constant G.W.L.. One of the reason of the difference might have been the shape and location of the slip surface. Figure 6a, b indicates the longitudinal shape of the surface (solid line) and slip surface (dashed line) in H21NIED model slope and H23NIED model slope. The location of the slip surface was at the foot of the slope section and the inclination of the slip surface was steep in H21NIED model slope. Steep slip surface at the foot of the slope section might have restricted the movement of landslide mass in the slope section and it might have made the creep behaviour under constant G.W.L. more significantly. The mechanism of the difference should be examined in future.

Relationship between the velocity and acceleration

The relationship between the velocity and acceleration is examined here for the prediction of failure time under repeated rainfall to demonstrate the influence of the rise in and lowering of the G.W.L. All the experimental periods are the target of this examination because the velocity did not increase monotonically and fluctuated, even immediately

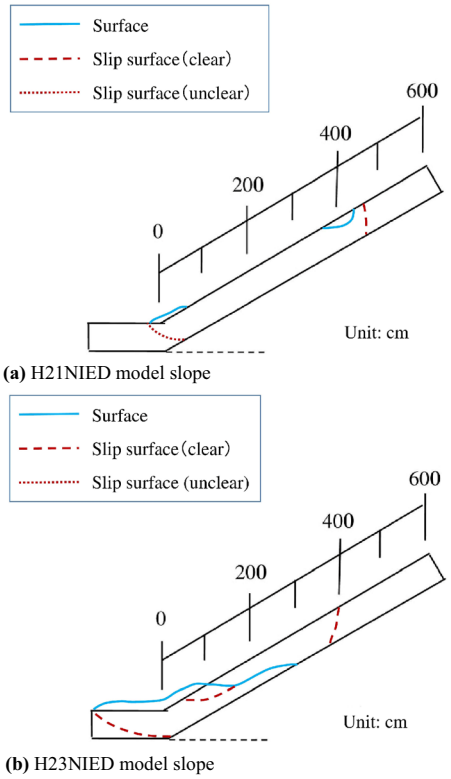

Fig. 6 The longitudinal shape and location of the slip surface in H21NIED and H23NIED model slope

before failure. Therefore, the tertiary creep stage (accelerating stage) could not have been easily defined in the experimental results. Positive and negative accelerations of the same magnitude were generated repeatedly according to the small fluctuation in the velocity, even immediately before failure. In the following analysis, positive acceleration was adopted when the surface displacement increased with the rise in the G.W.L. and negative acceleration was adopted when the surface displacement increased with the lowering of the G.W.L. because the velocity tended to increase during the significant rise in the G.W.L. Positive acceleration was also adopted when the surface displacement increased without a G.W.L. because the velocity tended to increase without G.W.L. during Rains 1 and 2, Stage I at 300 cm in the H21NIED model slope and during Rains 1 and 2, Stage I at 200 cm in the H23NIED model slope.

Figure 7a shows the relationship between the velocity and acceleration derived from the surface displacement at 300 cm from the toe of the H21NIED model slope. Positive acceleration was adopted in Stages I, II and IV, and negative acceleration was adopted in Stage III at 300 cm. In the figure, all the negative accelerations are shown as their absolute values. The relations in each stage can be expressed by unique lines at the logarithmic scale with 1 order of scatter in the absolute value of the acceleration. The data during the

latter half of Stage IV deviated from this line at both locations. The velocity remained near constant at approximately 0.01 cm/s with various accelerations. The video revealed that the soil mass moved at almost a constant velocity during these periods. Thus, the data reflect the movement of the soil mass after failure.

Figure 7b shows the relationships between the velocity and acceleration derived from the surface displacements at 200 cm from the toe of the H23NIED model slope. Positive acceleration was adopted in the period with the rise in and stabilisation of the G.W.L., while the absolute value of the negative acceleration was adopted in the period of G.W.L. lowering. The relationships in every stage can be expressed by a unique line at a logarithmic scale with small fluctuations. No large scatter in the final stage immediately before failure could be observed in this case.

In these experiments, the relationship between the velocity and the absolute value of the acceleration is represented by a single line on a logarithmic scale, regardless of the condition of the G.W.L. This means that the relationship was consistent during both the increase in velocity and decrease in velocity. This develops the utility of Eq. (1) not only for positive acceleration ($dv/dt > 0$) but also for negative acceleration ($dv/dt < 0$). This suggests that the relationship between the velocity and acceleration is unique throughout the displacement of the slope.

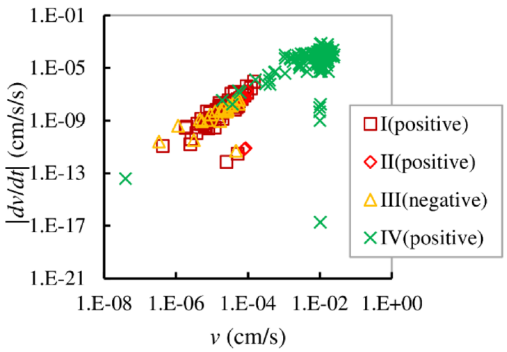

(a) 300 cm from the toe of the H21NIED model slope

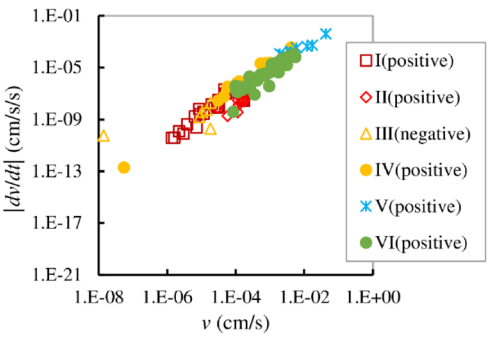

(b) 200 cm from the toe of the H23NIED model slope

Fig. 7 Relationship between the velocity and acceleration at **a** 300 cm from the toe of the H21NIED model slope and **b** 200 cm from the toe of the H21NIED model slope. *v* velocity. |*dv/dt*| absolute value of the acceleration

Table 3a shows the values of α and a for Eqs. (1) and (2), derived from the regression analysis of the relationship between the velocity and acceleration from the early stage to the start of the final stage (Stages I, II and III) at 300 cm from the toe of the H21NIED model slope for predicting the failure time at the final stage (Stage IV). Only data measured in the antecedent stage were used for the prediction at the final stage to validate the unique relationship between the velocity and acceleration. The value of α was 1.45 with the data at Stages I–III and around unity with the data at Stages II–III and Stage III with the determining factor ranging from 0.19 to 0.40 at 300 cm in the H21NIED model slope. The determining factor at 300 cm was lower due to the greater scatter of the acceleration at velocities from 1E-6 to 1E-4 in Fig. 7a for 300 cm.

Table 3b shows the values of α and a derived from the regression analysis of the relationship between the velocity and acceleration from the early stage to the start of the final stage at 200 cm from the toe of the H23NIED model slope. Durations for the analyses were from Stages I, II, III, IV and V to the start of Stage VI. The value of α ranged from 1.65 to 1.51 with a determining factor of 0.98 to 0.83 at 200 cm in the H23NIED model slope.

Scatter along the trendline for the relationship between the velocity and acceleration exhibit small differences in terms of the model constants α and a in regression equation representing Eq. (1). The relationship between the velocity and acceleration at different stages might essentially be unique, while the scatter due to the measurement error influences the value of the model constants in the regression equation. The value of the model constants varied slightly depending on the duration of the measurement. It is

Table 3 α, a and R^2 derived by the regression analysis for Eq. (1) of the relationship between the velocity and acceleration at (a) 300 cm from the toe of the H21NIED model slope and (b) 200 cm from the toe of the H23NIED model slope for predicting failure time at final stage

	α	*a*	R^2
(a) 300 cm from the toe of the H21NIED model slope			
Stages I–III	1.4543	−1.5399	0.3972
Stages II–III	0.9292	−4.1903	0.1863
Stage III	1.0651	−3.48	0.3359
(b) 200 cm from the toe of the H23NIED model slope			
Stages I–V	1.6462	−0.3749	0.8697
Stages II–V	1.5955	−0.4953	0.8345
Stages III–V	1.5149	−0.3585	0.9087
Stage IV–V	1.5603	−0.0752	0.9748
Stage V	1.5595	−0.1778	0.9756

important to determine the model constant α and a in Eq. (1) for predicting failure time in a series of rainfall events.

Fukuzono (1985) reported the linear relationship between velocity and acceleration on a logarithmic scale, as shown in Eq. (1), during tertiary creep in a model slope under constant rainfall. In this paper, the relationship expressed in Eq. (1) was proven to be accurate not only during the increase in the surface displacement velocity (tertiary creep) but also during the decrease in the surface displacement velocity. Moreover, a unique relationship between the velocity and acceleration could be established, even in different stages of repeated increases and decreases in the G.W.L., while model constants in the regression equation of Eq. (1) varied slightly depending on the duration of the measurement due to the scatter caused by measurement error. Thus, how to determine the duration of the data for precise prediction of the failure time of the slope should be examined.

Prediction of failure time

The relationship between the velocity and acceleration was derived at each location in both model slopes, and the corresponding constants a and α in Eqs. (1) and (2) were determined in a previous chapter. Now, the failure times in the H21NIED model slope and H23NIED model slope are predicted by Eq. (2) with the constants a and α in Table 3 to examine the influence of the difference in the duration of the measured data on the constants. The results at 300 cm in the H21NIED model slope and 200 cm in the H23NIED model slope are explained here. The results of the predicted failure time are examined with the value of α because the influence of α on the predicted failure time in Eqs. (1) and (2) is much greater than that of a.

Figure 8 shows the time variation in the predicted time derived by Eq. (2) and the constants a and α in Table 3a and the time remaining to failure during the final stage at 300 cm in the H21NIED model slope. The time remaining to failure is defined as the difference in the predicted failure time to the present time. The predicted failure times with different durations for the data were almost the same, ranging from 1,306,950 to 1,310,324 s, falling very closely to the present time. The time remaining to failure with the data at Stages II–III and Stage III was very small (− 10 s ~ 0 s), with an α of almost unity and a determining factor of less than 0.33. It could be considered almost zero throughout the period. This indicates that the predicted failure time was almost equal to the present time throughout the period, and it is not good for use in the prediction. While the time remaining to failure was − 200 s at 1,306,430 s at first and then smoothly approached around − 10 s until 1,308,580 s, it finally remained almost constant from 1,308,580 s to failure with measured data at Stages I–III. The value of α was 1.45,

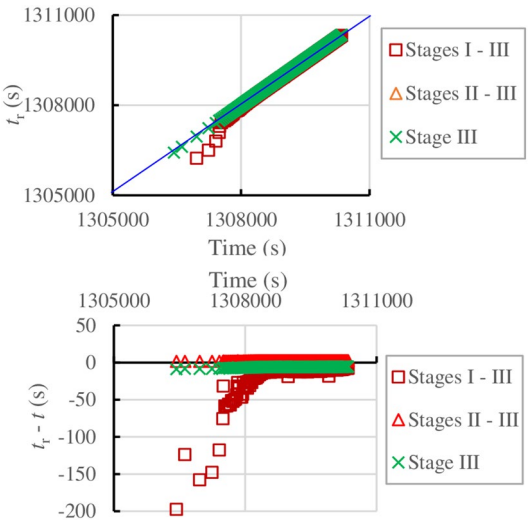

Fig. 8 The variations in the predicted failure time and the time remaining to failure derived from the model constants in Table 3(a) during Stage IV at 300 cm from the toe of the H21NIED model slope. t_r: predicted failure time. t_r–t: time remaining to failure. The blue line indicates that the present time is equal to the predicted failure time

and the determining factor was 0.40 for this case. It is good that the time remaining to failure smoothly approaches zero with time just prior to failure as the prediction. The time remaining to failure can be an indicator for prediction. A continuous decrease in the time remaining to failure indicates approaching the failure time.

Figure 9 shows the time variation in the predicted failure time derived by Eq. (2), the constants a and α in Table 3b and the time remaining to failure during the final stage at 200 cm in the H23NIED model slope. The predicted failure time approached the present time with advancing time and then converged to almost the same value at the actual failure time (1,478,655 s), even though the time remaining to failure varied from − 6000 to − 800 s at the start of the final stage (1,476,165 s). The time remaining to failure smoothly approached near zero with time until failure. It is good for the prediction. Thus, the model constants a and α with any duration of measured data can be adopted for the prediction. Any data with different durations produced a value of α of 1.5–1.65 with a determining factor of more than 0.83 in this case.

It was recognised that an α value of more than approximately 1.45 with a determining factor of more than 0.40 could make good predictions for early warning. The time remaining to failure smoothly approached zero with time until failure with this value. This indicates that the result of the predicted failure time might be better with a high value of α and a high determining factor. The duration of the measured data with a high value of α and a high determining factor should be selected for the prediction in cases of

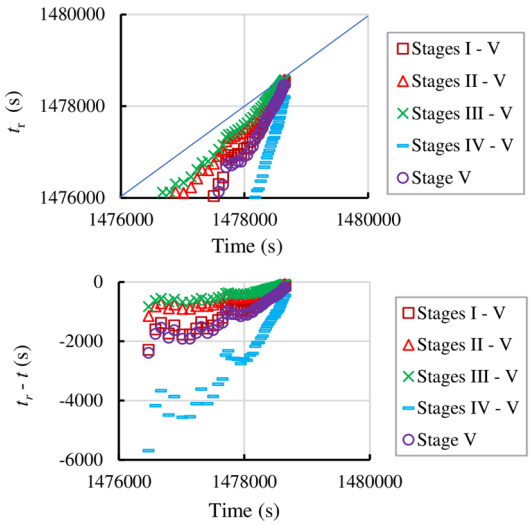

Fig. 9 The variations in the predicted failure time and the time remaining to failure derived from the model constants in Table 3(b) during Stage VI at 200 cm from the toe of the H23NIED model slope. t_r: predicted failure time. t_r–t: time remaining to failure. The blue line indicates that the present time is equal to the predicted failure time

repeated rainfall before the final event. Data measured not only during the period with increasing velocities but also with decreasing velocities can be used to derive a regression equation representing Eq. (1). The time remaining to failure approaching zero could be recognised as an indicator for the failure of the slope; the sign of the values might not be important.

Conclusion

Analyses of the measured data of the pore pressure and deformation of a sandy model slope under repeated rainfall events were performed to reveal the effect of the repeated loading and unloading of pore pressure on the slope deformation. The velocity and acceleration were derived from the surface displacement measured in the slope. The results are as follows:

1. The velocity fluctuated and did not undergo a monotonic increase, even immediately before failure. No period with a constant velocity (secondary creep) or monotonic increase in velocity (tertiary creep) was observed in the experiment. This was due to the repeated small increases and decreases in the surface displacement. Positive and negative accelerations appeared alternately in accordance with the fluctuation in the velocity. The magnitude of the negative acceleration was almost the same as that of the positive acceleration.
2. The surface displacement increased not only with the rise in the G.W.L. but also with the lowering and stabilisation of the G.W.L. The variation in the surface displacement with the lowering of the G.W.L. was due to the delay in the water seepage.
3. The relationship between the velocity and the absolute value of the acceleration derived from the surface displacement was unique for not only the period of increasing velocity but also the period of decreasing velocity according to the variation in G.W.L. owing to repeated rainfall, except for the stage during and after failure. The relationships were linear on a logarithmic scale. Note that these relationships were the same under an increasing, a decreasing and a constant G.W.L., without considering the point after failure.
4. The constants for the equation used to predict the failure time in the slope proposed by Fukuzono were derived by linear regression analysis of the relationship between the velocity and acceleration during different periods before the final stage at 300 cm in the H21NIED model slope and at 200 cm in the H23NIED model slope. The prediction of failure time was implemented by the equation and the time remaining to failure, which was defined as the difference between the present time and predicted failure time was derived. The results show that the time remaining to failure approached a constant value close to zero at the actual time of failure, when the constants were derived with a high value of α and a high determining factor. It is good for the prediction of failure time as an early warning metric. The data measured not only during the period with increasing velocities but also that with decreasing velocities can be used to derive the constants. The time remaining to failure approaching zero might be a useful indicator for predicting the failure time.

These results improve the utility of the relationship proposed by Fukuzono (1985) from being applicable during only a positive acceleration to being applicable during the entire test with increasing surface displacement. This might allow the earlier prediction of the failure time of a slope with the Fukuzono method because the measured data not only immediately before the failure (tertiary creep) but also during the earlier stage of deformation could be used for the prediction.

Funding Part of this research is supported by the Grant-in-Aid for Scientific Research B -KAKENHI-, 18H01674, JSPS.

Data availability Data in this paper are not available.

Declarations

Conflict of interest The author declares that they have no competing interests.

References

Abraham MT, Satyam N, Bulzinetti MA, Pradhan B, Pham BT, Segoni S (2020) Using field-based monitoring to enhance the performance of rainfall thresholds for landslide warning. Water 12:3453. https://doi.org/10.3390/w12123453

Bozzano F, Mazzanti P (2012) Assessing of failure prediction methods for slope affected by human activities, In: Eberhardt E, Froese C, Turner AK, Leroueil S (Eds.) Landslides and Engineered Slopes: Protecting Society through Improved Understanding (Proc of 11th Int. and 2nd North American symposium on landslides and Engineered Slopes, Banff, Canada, 3–8 June 2012). CRC Press/Balkema, Leiden, pp.1465–1471.

Carlà T, Nolesini T, Solari L, Rivolta C, Cas LD, Casagri N (2019) Rockfall forecasting and risk management along a major transportation corridor in the Alps through ground-based radar interferometry. Landslides 16:1425–1435. https://doi.org/10.1007/s10346-019-01190-y

Crosta GB, Agliardi F (2003) Failure forecast for large rock slides by surface displacement measurements. Can Geotech Jour 40:176–190

Fukuzono T (1985) A New Method for Predicting the Failure Time of a Slope. In: Proceedings of the 4th International Conference and Field Workshop on Landslides, Tokyo, Japan, pp.145–150.

Hao S, Liu C, Lu C, Elsworth D (2016) A relation to predict the failure of materials and potential application to volcanic eruptions and landslides. Sci Rep 6:27877. https://doi.org/10.1038/srep27877

Hao S, Yang H, Elsworth D (2017) An accelerating precursor to predict "time-to-failure" in creep and volcanic eruptions. J Volcanol Geoth Res 343:252–262. https://doi.org/10.1016/j.jvolgeores.2017.07.009

Intrieri E, Gigli G, Mugnai F, Fanti R, Casagli N (2012) Design and implementation of a landslide early warning system. Eng Geol 147–148:124–136. https://doi.org/10.1016/j.enggeo.2012.07.017

Iwata N, Sasahara K, Watanabe S (2017) Improvement of Fukuzono's model for time prediction of an onset of a rainfall-induced landslide. In: Mikos M et al (eds) Advancing culture of living with landslides. Springer International Publishing AG, Gewerbestrasse, pp 103–110

Loew S, Gschwind S, Gishig V, Keller-Signer A, Valenti G (2017) Monitoring and early warning of the 2012 Preonzo catastrophic rockslope failure. Landslides 14:141–154. https://doi.org/10.1007/s10346-016-0701-y

Mazzanti P, Bozzano F, Cipriani I, Prestininzi A (2015) New insights into the temporal prediction of landslides by a terrestrial SAR interferometry monitoring case study. Landslides 12:55–68. https://doi.org/10.1007/s10346-014-0469-x

Qiao S, Feng C, Yu P, Tan J, Uchimura T, Wang L, Tang J, Shen Q, Xie J (2020) Investigation on surface tilting in the failure process of shallow landslides. Sensors 20:2662. https://doi.org/10.3390/s20092662

Saito M (1965) Forecasting the time of occurrence of a slope failure. In: Proceedings of 6th International Conference on Soil Mechanics and Foundation Engineering, 2nd edn. Montreal, Canada, pp 537–541

Saito M, Yamada G (1973) Forecasting and Result in Case of Landslide at Takabayama. In: Proceedings of 8th International Conference on Soil Mechanics and Foundation Engineering, Moscow, U.S.S.R. 4(3), pp.325–327

Sasahara K, Sakai N (2017) Shear and compression strain development in sandy model slope under repeated rainfall. Soils Found 57:920–934. https://doi.org/10.1016/j.sandf.2017.08.021

Uchimura T, Suzuki D, Hongkwan S (2011) COMBINED MONITORING OF WATER CONTENT AND DISPLACEMENT FOR SLOPE INSTABILTY. In: Proceedings of 4th Japan-Korea Geotechnical Engineering Workshop, Japanese Geotechnical Society, Kobe, pp.67–72

Varns DJ (1982) Time-deformation relations in creep to failure of earth materials. In: Proceedings of 7th Southeast Asian Geotechnical Conference 2, pp.107–130

Voight B (1988) A relation to describe rate-dependent material failure. Science 243:200–203

Voight B (1989) Materials science law applies to time forecasts of slope failure: In: Japan Landslide Society (Eds) Landslide news, Tokyo, 3:8–10

Xiao J-Q, Ding D-X, Xu G, Jiang F-L (2009) Inverted S-shaped model for nonlinear fatigue in rock. Int J Rock Mech Mining Sci 46:643–548

Xie J, Uchimura T, Wang G, Shen Q, Maqsood Z, Xie C, Liu J, Lei W, Tao S, Chen P, Dong H, Mei G, Qiao S (2020) A new prediction method for the occurrence of landslides based on the time history of tilting of the slope surface. Landslides 17:301–312. https://doi.org/10.1007/s10346-019-01283-8